Correspondence Between Behavioral, Physiological, and Anatomical Measurements of Visual Function in Inhibitory Neuron–Ablated Zebrafish

Jiaheng Xie,[1] Patrick T. Goodbourn,[2] Bang V. Bui,[3] Tamar E. Sztal,[4] and Patricia R. Jusuf[1]

[1]School of Biosciences, The University of Melbourne, Melbourne, Australia
[2]Department of Optometry and Vision Sciences, The University of Melbourne, Melbourne, Australia
[3]Melbourne School of Psychological Sciences, The University of Melbourne, Melbourne, Australia
[4]School of Biological Sciences, Monash University, Melbourne, Australia

Correspondence: Patricia R. Jusuf, School of Biosciences, Building 184, Room 333, The University of Melbourne, Melbourne, Victoria 3010, Australia;
patricia.jusuf@unimelb.edu.au.

Submitted: May 23, 2019
Accepted: October 5, 2019

Citation: Xie J, Goodbourn PT, Bui BV, Sztal TE, Jusuf PR. Correspondence between behavioral, physiological, and anatomical measurements of visual function in inhibitory neuron–ablated zebrafish. *Invest Ophthalmol Vis Sci*. 2019;60:4681–4690. https://doi.org/10.1167/iovs.19-27544

Purpose. To compare the effects of reduced inhibitory neuron function in the retina across behavioral, physiological, and anatomical levels.

Methods. Inhibitory neurons were ablated in larval zebrafish retina. The *Ptf1a* gene, which determines inhibitory neuron fate in developing vertebrates, was used to express nitroreductase. By exposing larvae to the prodrug metronidazole, cytotoxicity was selectively induced in inhibitory neurons. Visual phenotypes were characterized at behavioral, physiological, and anatomical levels using an optomotor response (OMR) assay, electroretinography (ERG), and routine histology, respectively. Nonvisual locomotion was also assessed to reveal any general behavioral effects due to ablation of other nonvisual neurons that also express *Ptf1a*.

Results. Injured larvae showed severely reduced OMR relative to controls. Locomotor assessment showed unaltered swimming ability, indicating that reduced OMR was due to visual deficits. For ERG, injured larvae manifested either reduced (type-I) or absent (type-II) b-wave signals originating from bipolar interneurons in the retina. Histologic analysis showed altered retinal morphology in injured larvae, with reductions in synaptic inner plexiform layer (IPL) thickness and synaptic density more pronounced in type-II than type-I larvae; type-II larvae also had smaller retinae overall.

Conclusions. The consequences of inhibitory neuron ablation corresponded closely across behavioral, physiological, and anatomical levels. Inhibitory neuron loss likely increases the ratio of neural excitation to inhibition, leading to hyperexcitability. In addition to modulating visual signals, inhibitory neurons may be critical for maintaining retinal structure and organization. This study highlights the utility of a multidisciplinary approach and provides a template for characterizing other zebrafish models of neurological disease.

Keywords: retina, optomotor, electoretinography, analysis pipeline

The zebrafish *(Danio rerio)* is a compelling vertebrate model for visual neuroscience. Owing to its high conservation of genetics and retinal structure with other vertebrate species, the zebrafish is ideal for investigating visual development and eye genetics, modeling human ocular diseases, and drug discovery.[1–5] During larval stages, zebrafish rely primarily on visual perception for evading predators and capturing prey, selectively driving rapid maturation of the visual system.[6]

The visual system is arguably the best characterized and most easily probed neural system, as it can be readily assessed at multiple levels including behavior, physiology, and histology. In addition to well-described histologic techniques, the behavioral optomotor response (OMR) and functional electroretinogram (ERG) are also increasingly used in studies of zebrafish vision.[7–14] The OMR is an innate, visually guided behavior that can be elicited as early as 4 days post fertilization (dpf),[15] and is often exploited in the lab to screen for visual deficits, measure motion perception, or characterize chromatic and spatiotemporal response properties of the visual system.[7,8,16,17] Unlike the OMR, which captures visual function across the central nervous system (CNS) as a whole, the ERG assesses neural function specifically in the retina. When visual input is detected and processed in the retina, electrical currents are generated and transferred to the central corneal surface, where they can be detected using the ERG.[18] The most commonly analyzed ERG components are the a-wave and b-wave, generated by light-sensing photoreceptors and bipolar cells, respectively. The ERG is an important tool for assessing visual function, color vision, circadian rhythms, normal development, and drug response.[11–15] Together, these well-established tools allow multilevel analysis of the visual system.

Inhibitory neurons play vital roles throughout the CNS. For example, reduced inhibitory synaptic transmission in mice leads to an imbalanced ratio of neural excitation to inhibition (E/I), and thus hippocampal hyperexcitability.[19] Inhibitory neuron deficits in the human brain are implicated in neurodevelopmental disorders including autism spectrum disorders, schizophrenia, and epilepsy.[20–23] In the retina,

inhibitory neurons include horizontal and amacrine interneurons. Horizontal cells in the outer retina modulate signaling between photoreceptors and bipolar cells, contributing to color vision, adjusting bipolar cell and ganglion cell receptive field size, and contributing to gain control.[24–28] Amacrine cells in the inner retina modulate signaling between bipolar cells and ganglion cells or transmit signals to other amacrine cells, contributing to spatiotemporal processing of moving stimuli and selective signal amplification.[29,30] A wide variety of subtypes of each are involved in more specialized visual modalities. For instance, dopaminergic amacrine cells release dopamine depending on luminance levels to uncouple gap junctions for both horizontal and amacrine cells, narrowing their receptive fields and the amplitude of light responses.[24,31,32] Retinal inhibitory neurons are thus critical to normal visual processing.

Here, we used a transgenic zebrafish line Tg(*ptf1a*:*Gal4*/*UAS*:*nfsb-mCherry*) with nitroreductase-mediated cell ablation to selectively ablate inhibitory neurons,[33] based on the spatiotemporal expression of the pancreas-specific transcription factor 1a (Ptf1a).[34] *Ptf1a* is a basic helix-loop-helix (bHLH) transcriptional gene that determines inhibitory neuron fate in many regions of the CNS including the retina, and is transiently expressed in developing zebrafish.[35–38] We measured ERG and OMR for inhibitory neuron–ablated larvae to analyze visual behavior and function. Our primary aim was to assess the correspondence between behavioral (OMR), physiological (ERG), and anatomical (histology) findings. Using general locomotor testing we could also assess whether the OMR was affected by ablation of nonvisual inhibitory neurons across the CNS.

Methods

Animal Husbandry

Zebrafish *(Danio rerio)* were maintained and bred in the Fish Facility at the Walter and Eliza Hall Institute of Medical Research according to local animal guidelines. Embryos of either sex were grown at 28.5°C and staged in dpf. Tg(*ptf1a*:*Gal4*/*UAS*:*nfsb-mCherry*) larvae were randomly assigned to experimental groups. All procedures were performed based on the provisions of the Australian National Health and Medical Research Council code of practice for the care and use of animals in research, adhered to the ARVO Statement for the Use of Animals in Ophthalmic and Vision Research, and were approved by Faculty of Science Ethics Committee at the University of Melbourne.

Genetic Ablation of Inhibitory Neurons

The model of inhibitory neuron ablation was adapted from previous studies.[33,34] In Tg(*ptf1a*:*Gal4*/*UAS*:*nfsb-mCherry*) larvae, Gal4 expression is driven by the *Ptf1a* promotor to bind the activating sequence UAS, leading to the production of the nitroreductase enzyme and the red fluorescent reporter mCherry. Expression is restricted to inhibitory neurons, as *Ptf1a* determines inhibitory fate in the developing vertebrate CNS.[39] Upon exposure to metronidazole, nitroreductase converts metronidazole into cytotoxin in inhibitory neurons, resulting in rapid neuronal ablation, as we previously characterized.[34] Here, 3 dpf Tg(*ptf1a:Gal/UAS:nfsb-mCherry*) embryos were immersed in 8 mM metronidazole/0.1% dimethyl sulfoxide (DMSO) dissolved in egg water (60 mg/L sea salt) for 16 hours overnight at 28.5°C. Embryos were then rinsed and raised in egg water until 7 dpf, when the effect of the ablation is maximal following this treatment, and prior to the start of functional regeneration.[34] Control fish were transgenic larvae treated with 0.1% DMSO only.

Optomotor Response

Apparatus and Procedure. The OMR apparatus was adapted from one previously described.[10] Larvae ($n = 50 \pm 5$ in each group) were contained in a five-lane arena with a transparent base (Supplementary Fig. S1). Gaussian noise textures, filtered to achieve center spatial frequencies of 0.005, 0.01, 0.02, 0.04, 0.08, 0.16, or 0.32 c/° (SD = 0.5 octaves), were displayed below the arena at full contrast. During a trial, the textures drifted at 25, 50, or 100 °/s parallel to the long axis of the lanes. Before experiments, larvae were transferred to arena lanes within 10 minutes, after which they were allowed to adapt to the arena for 10 minutes. Prior to each trial, a corralling stimulus was shown for 30 seconds to guide larvae to the center of the lane. This was followed by a 30-second presentation of a test stimulus. A camera controlled by a custom MATLAB (MathWorks, Natick, MA, USA) program captured images before and after each trial for calculation of swimming distance. A blank gray screen was presented after the offset of the test stimulus while the texture for the next trial was computed. Injury and control groups performed 28 and 21 trials, respectively, per combination of spatial frequency and speed. All experiments were conducted between 9:30 AM and 6:00 PM.

Image Analysis. Larval positions were extracted from the before and after images for each trial using a custom MATLAB algorithm. Image contrast was flattened, and a Laplacian of Gaussian filter was applied to highlight edges.[40] Larvae were segmented by thresholding, and the centroid of larval positions was calculated using bwconncomp and regionprops commands from the MATLAB Image Processing Toolbox. On each trial, the change in position of the centroid in the direction of texture motion was computed as the OMR index. Normalized optomotor indices were calculated by normalizing all data to the OMR index of control larvae for 0.02 c/° stimuli drifting at 25 °/s. The contrast sensitivity function (CSF) was a log-Gaussian fitted to the data using a least-squares criterion. For each fitted model, the estimated parameters were amplitude (i.e., height of the peak), peak frequency (i.e., spatial frequency at which amplitude peaked), and bandwidth (i.e., standard deviation). To determine whether CSFs differed between groups, we used an omnibus *F*-test to compare a full model, in which each group's parameter estimates could vary independently, with a restricted model, in which parameters were constrained to be the same across groups. Further, to determine whether estimates of specific parameters differed between groups, we used an *F*-test to compare the full model to a restricted model in which one parameter was constrained to be the same across groups.[41] We used a criterion of $\alpha = 0.05$ to determine significance, with Bonferroni correction applied to *P* values to account for multiple testing.

Locomotor Response

The locomotor assay was adapted from a previously published method.[42] Larvae were randomly assigned to individual wells in 24-well dishes. Locomotion was quantified under 10 minutes of dark in E3 medium, or in 1.5% ethanol in E3 medium with exposure commencing 5 minutes prior to testing. Locomotion was recorded and analyzed using the Zebrabox system and Zebralab software (Viewpoint Life Sciences, Inc., Lyon, France) with an infrared digital camera above the plates. An inactivity threshold of 1 mm/s, detection threshold of 30 mm/s, and maximum burst threshold of 30 mm/s were applied. The total swimming distance and duration within these thresholds were

extracted, and data were normalized to the swimming performance of the control group within each assay. Statistical analysis was performed in Prism 7.0 (GraphPad Software Inc., San Diego, CA, USA), with Mann-Whitney tests or unpaired *t*-tests ($\alpha = 0.05$) applied, depending on the normality of data according to a Shapiro-Wilk test. Outliers were excluded using the ROUT method ($Q = 1\%$). There were between 51 and 88 larvae per group (see Supplementary Information for further details).

Electroretinography

Larval scotopic ERG was measured using a previously published method.[15] All experiments were performed between 9:00 AM and 6:00 PM at room temperature. Larvae were dark adapted overnight (>8 hours) before measurements. Larvae were readapted in complete darkness for >3 minutes after the placement of electrodes under dim red light. We used flash intensities of −2.11, −0.81, 0.72, 1.89, and 2.48 log cd.s/m^2. Interstimulus intervals increased with intensity from 10 to 60 seconds. We made one to three recordings per intensity (depending on signal-to-noise ratio) from 11 control and 17 injury-model larvae. The amplitude of ERG signals was extracted using Microsoft Excel (ver. 16.16.3; Microsoft, Redmond, WA, USA). For larvae with visible b-waves, amplitude was measured from the negative a-wave trough to the positive b-wave peak. For larvae lacking b-waves, amplitude was measured at the negative trough. After experiments, larvae were euthanized using 0.1% tricaine and fixed for histologic analysis. Data were analyzed (Prism 7.0) using 2-way ANOVA with Tukey control for multiple comparisons ($\alpha = 0.05$).

Histology

Immunohistochemistry. Zebrafish embryos were fixed in 4% paraformaldehyde (PFA) in phosphate-buffered saline (PBS), cryoprotected in 30% sucrose, embedded in optimum cutting temperature (Tissue-Tek, Miami, FL, USA), and cryostat sectioned at 12-µm thickness. All antibody staining was performed at room temperature using standard protocols. For antigen retrieval, slides were incubated in boiled 10 mM sodium citrate (pH 6) until the solution was cooled to room temperature. To quantify synaptic distribution, we labeled for postsynaptic density 95 (PSD-95), as this protein strengthens postsynaptic proteins across the CNS[43] and can be used as a general marker of synapses. Slides were blocked in 5% fetal bovine serum (FBS) for 30 minutes and incubated overnight in rabbit anti-PSD-95 antibody (1:100; Abcam, Cambridge, UK; cat. number ab18258) diluted in 5% FBS. Slides were subsequently rinsed in PBS and incubated for 2 hours in anti-rabbit Alexa Fluor 488 (1:500; Thermo Fisher Scientific, Waltham, MA, USA; cat. number A11001) diluted in 5% FBS. Nuclei were stained with 4′,6-diamidino-2-phenylindole (DAPI; 1:10,000; Sigma-Aldrich, St. Louis, MO, USA; cat. number D9542-10MG) in PBS for 20 minutes and sections were mounted in Mowiol (Sigma-Aldrich, cat. number 81381-250G).

Image Acquisition. Retinal sections were imaged using a ZEISS Axioscope (Carl Zeiss Microscopy GmbH, Oberkochen, Germany; ×20 or ×100 objective lens). For observation of PSD-95 puncta, images were captured using a ×100 objective lens with the ApoTome system. For quantification of retinal size and inner plexiform layer (IPL) thickness, images were taken within two sections from the optic nerve. Image brightness and contrast were adjusted using Photoshop (Adobe, San Jose, CA, USA) or FIJI.[44]

Image Analysis. For retinal size quantification, the polygon selection in FIJI was used to outline the retina and measure the size of the selected area. IPL thickness was also measured with FIJI, defined as the average of the thickness at the central IPL and at 45° in each direction. Retinal size and IPL thickness data were normalized to control larvae. To determine the number of *Ptf1a*-positive (*Ptf1a*+) neurons, cells were counted manually and standardized to 400 µm, corresponding to the length of the retina in an average retinal section. Statistical analysis was performed in Prism 7.0 using 1-way ANOVA ($\alpha = 0.05$). There were 10 control and 20 injury-model retinae, with the latter comprising two distinct groups of 10 as defined by ERG (see Results).

Results

Optomotor Response

We measured the CSF using OMR in control ($N = 21$ trials per combination of spatial frequency and speed) and injured larvae ($N = 28$ trials per combination). All CSFs were well described by a spatially bandpass log Gaussian model (Figs. 1a–c). An omnibus test indicated that at each speed, overall CSFs differed between groups ($P = 0.018$, $P = 0.041$, and $P = 0.002$ for 25, 50, and 100 °/s, respectively; Figs. 1a–c; Supplementary Table S1). Examining individual parameters of the CSF, amplitude (i.e., the height of the CSF peak) at each speed was higher for control than for injured larvae ($P = 0.011$, $P = 0.011$, and $P = 0.021$ for 25, 50, and 100 °/s, respectively; Fig. 1d). Cell ablation had no discernible effect on peak frequency (i.e., the spatial frequency at which amplitude peaked) at any stimulus speed (Fig. 1e). Bandwidth (i.e., the standard deviation of the CSF) was higher for control than for injured larvae, but only at 100 °/s ($P = 0.043$; Fig. 1f). Overall, compared to the control fish, OMR was significantly impaired in inhibitory neuron–ablated larvae.

Locomotor Response

Since OMR requires coordination between tissues throughout the CNS (where *Ptf1a* expression is conserved across inhibitory neuron populations),[36–38] we tested the general swimming performance of injured larvae to rule out a motor deficit. Unexpectedly, injured larvae ($N = 72$) spontaneously swam longer distances than control larvae ($N = 71$; $P = 0.032$; Fig. 2a). Normalized swimming speeds were not discernibly different between the two groups ($N = 70$ for controls and $N = 72$ for injured larvae; Fig. 2b; Supplementary Table S2). These results suggested that ablation of inhibitory neurons did not reduce general swimming ability.

Inhibitory neurons are also found in the cerebellum, which contributes to locomotion. Cerebellar function was thus assessed using ethanol exposure, which can cause cerebellar dysfunction in humans,[45] and intermediate doses of ethanol cause hyperactivity in larval zebrafish.[46] Our results revealed no difference in swimming distance between control and injured larvae following ethanol exposure ($N = 51$ and $N = 88$, respectively; Fig. 2c; Supplementary Table S2), although injury significantly increased swimming speed ($N = 52$ for control larvae and $N = 88$ for injured larvae; $P = 0.018$; Fig. 2d). These results implied that the cerebellum-mediated effect of ethanol on larval motor response is not abolished in injured fish. Thus, the effects of neural ablation on OMR are unlikely due to motor or cerebellar dysfunction.

Electroretinography

Scotopic ERG of injured larvae revealed that although there is variability between eyes, the pattern of b-wave loss appears to fall into two distinct groups, with either a reduced or an absent

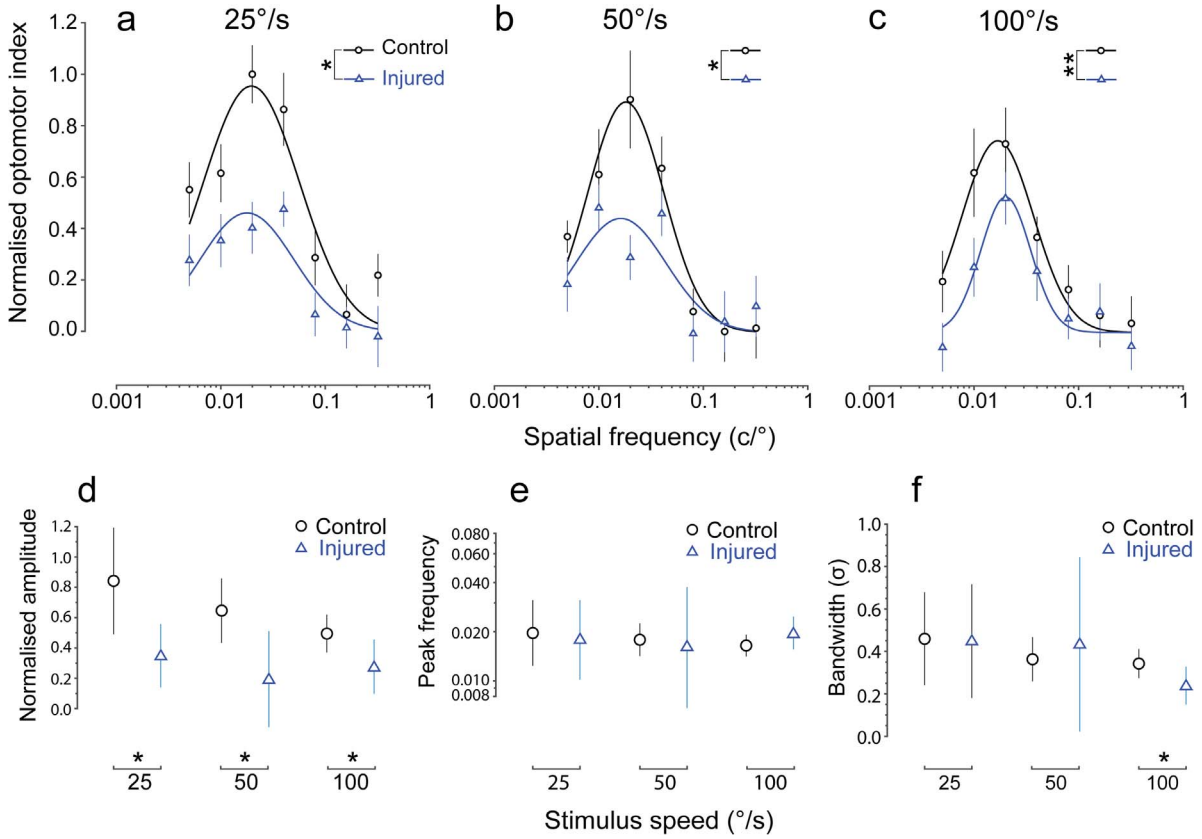

FIGURE 1. Contrast sensitivity functions from the OMR of control and injured larvae. The *upper row* shows CSFs for control (*black circles*) and injured larvae (*blue triangles*) at (**a**) 25, (**b**) 50, and (**c**) 100 °/s. *Lines* show the three-parameter log-Gaussian function providing best fit to the data in a least-squares sense. *Asterisks* in the *upper row* indicate significant overall differences in CSF between groups at each speed. *Error bars* show ± SEM across trials. The *bottom row* shows (**d**) normalized amplitude, (**e**) peak spatial frequency, and (**f**) bandwidth as a function of group and stimulus speed. *Error bars* show the 95% confidence intervals on the fitted parameters. $^{*}P < 0.05$; $^{**}P < 0.01$.

b-wave at all intensities (Fig. 3a; Supplementary Fig. S2); we refer to these as type-I and type-II larvae, respectively. Note that while the large b-wave component actually appears inverted in type-II larvae, this represents negative-polarity components of the signal that are revealed in the absence of the b-wave, as is the case for mouse mutants with postsynaptic defects.[47] ERG amplitudes for each intensity were also quantified from the negative trough of the a-wave to the positive peak of the b-wave peak (around 70 ms post stimulus onset) for control ($N = 11$) and type-I larvae ($N = 11$), and at the trough of the signal for type-II larvae ($N = 6$). Amplitudes for control larvae were significantly higher than for both type-I and type-II injured larvae at intensities of 0.72, 1.89, and 2.48 log cd.s/m^2 ($P < 0.0001$ for each intensity). In comparison to type-II injured larvae, control larvae also showed significantly higher amplitudes at all tested stimulus intensities ($P = 0.03$ for –2.11 log cd.s/m^2 and $P < 0.0001$ for others). Additionally, at intensities of –0.81 log cd.s/m^2 or higher, type-I larvae had significantly higher amplitudes than type-II larvae ($P < 0.0001$ for all; Fig. 3b; Supplementary Table S3).

Histology

In order to identify anatomical substrates of our behavioral and physiological phenotypes, we quantified cell loss, retinal size, IPL thickness, and synaptic distribution within the retina. Having characterized the ERG responses prior to histologic analysis, we could also compare anatomical properties of type-I and type-II larvae.

As expected, our quantification showed a significant reduction of *Ptf1a*+ inhibitory cells for type-I and type-II injured compared to control larvae ($N = 10$ per group; both $P < 0.0001$; Figs. 4a–d; Supplementary Tables S4, S5), but there was no evidence of a difference between the two injured types. While retinal size was comparable between control and type-I injured groups, type-II larvae showed significantly smaller retinae than other groups ($N = 10$ per group; both $P < 0.0001$; Figs. 4a′–a‴, 4b′–b‴, 4c′–c‴, 4e; Supplementary Tables S4, S5). Both type-I and type-II injured larvae had significantly thinner IPL than control larvae ($N = 10$ per group; $P = 0.0013$ and $P < 0.0001$, respectively); reductions in type-II were more severe than in type-I larvae ($P < 0.0001$; Fig. 4f; Supplementary Tables S4, S5).

Both injured types also showed reduced synaptic density, which was more severe in type-II than in type-I. With highly reduced IPL thickness, all 12 sampled type-II retinae showed no PSD-95 puncta or markedly fewer puncta than controls; by comparison, this occurred in only 8 of 16 samples for type-I larvae (Figs. 4a*, 4b*, 4c*; Supplementary Table S5). Overall, these results revealed that the anatomical deficits in type-II injured larvae were more severe than in type-I larvae, mirroring the inner retinal b-wave phenotype in ERG.

DISCUSSION

Multilevel analysis including OMR, ERG, and histology provides mechanistic insight into how inhibitory neuron loss affects visual processing at behavioral, physiological, cellular, and

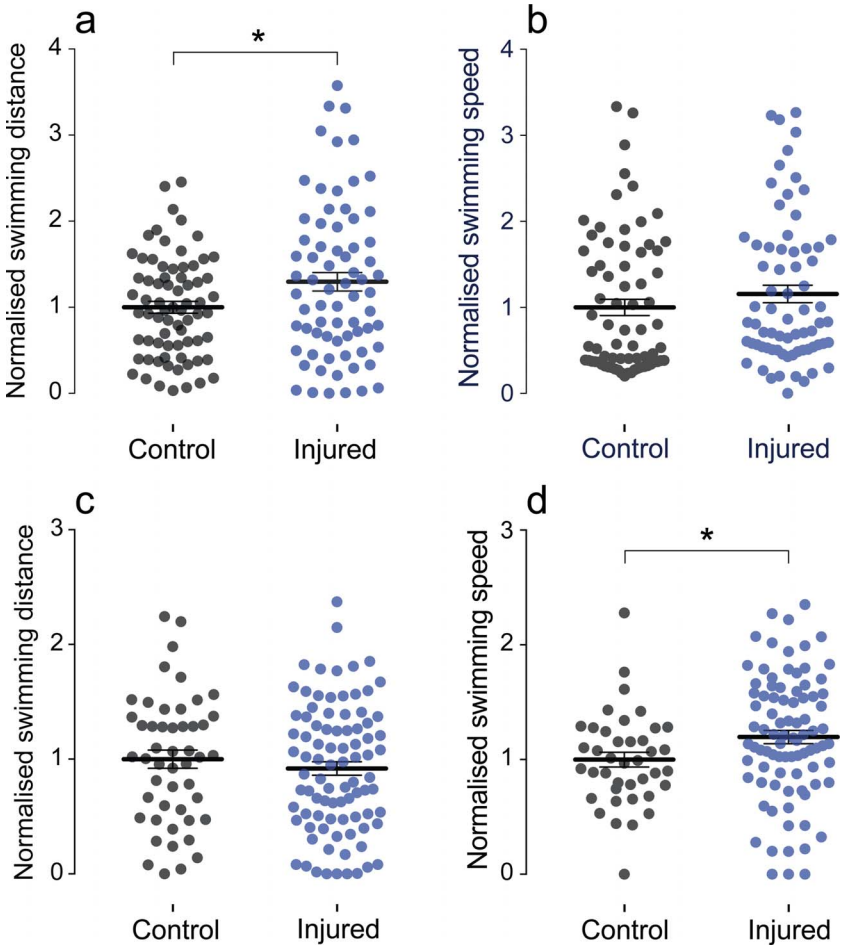

FIGURE 2. Locomotor responses of control and injured larvae. (**a**) Normalized swimming distances and (**b**) swimming speeds for control and injured larvae under 10-minute dark conditions in E3 medium. (**c**) Normalized swimming distances and (**d**) swimming speeds for control and injured larvae under 10-minute dark conditions in 1.5% ethanol. *Black* and *blue points* are individual control and injured larvae, respectively. *Error bars* show ± SEM. $^{*}P < 0.05$.

synaptic levels. Ablation of inhibitory neurons resulted in retinal morphologic disorganization and a reduction in synaptic density, causing disrupted physiological signaling and leading to abnormal visual behavior. Anatomical analysis revealed different levels of reduction in retinal and IPL size, and in IPL synaptic density, between larvae that had reduced (type-I) versus absent (type-II) ERG b-waves, demonstrating a correspondence between physiological and histologic results. The altered CSF indexed by OMR also revealed deficits in injured larvae, consistent with ERG and histologic findings. However, as a group-based assay, our OMR measure did not differentiate between type-I and type-II ERG injury phenotypes. Based on the ERG and histology phenotypes, we suspect that if type-I and type-II injured larvae were separated prior to OMR assessment, there may be a more striking difference in OMR performance in fish with an absent b-wave.

Locomotor results indicated that impaired visual function was likely the primary cause of reduced OMR in injured larvae. There was no general impairment of motor swimming ability. However, in zebrafish, generation of the OMR also involves nonretinal visual neurons in pretectum.[48] It thus remains possible that injury to inhibitory neurons outside the eye (e.g., pretectum)[49] also contributes to the observed OMR deficits.

Many studies have emphasized the importance of E/I balance for normal behavior,[50–53] and an increased E/I ratio has been implicated in a range of psychological disorders including autism spectrum disorder, schizophrenia, and attention-deficit hyperactivity disorder.[22,23,54,55] Neuronal overexcitation in mice can give rise to motor hyperactivity and enhanced exploratory behaviors.[56] In our study, injured larvae were indeed more active than control larvae in locomotor tests, likely because an increased E/I ratio resulted in motor hyperactivity. Further work using pharmacological treatments to modulate excitatory glutamatergic transmission in injured larvae (e.g., autotoxin inhibition for reducing brain hyperexcitability)[50] could confirm the contribution of E/I imbalance to our locomotor phenotype.

Our results suggest that in addition to modulating visual signals, the inhibitory horizontal cells may also serve to stabilize bipolar cell dendrites in the photoreceptor terminal and maintain physiological integrity in the outer plexiform layer (OPL).[57,58] In adult mice, selectively ablating horizontal cells using the diphtheria toxin (DT)/DT-receptor system and connexin57 promoter resulted in altered ERG a- and b-waves, lower visual acuity and contrast sensitivity, rod photoreceptor degeneration, and retinal remodeling.[59] After horizontal cell ablation, only cone (not rod) photoreceptors survived, and these preserved contacts only with OFF-bipolar cells.[59] The synaptic connections between photoreceptors, ON-bipolar cells, and horizontal cells were lost, suggesting that changes in the ON-pathway caused the altered ERG response in that study. In the present study, horizontal cell numbers declined

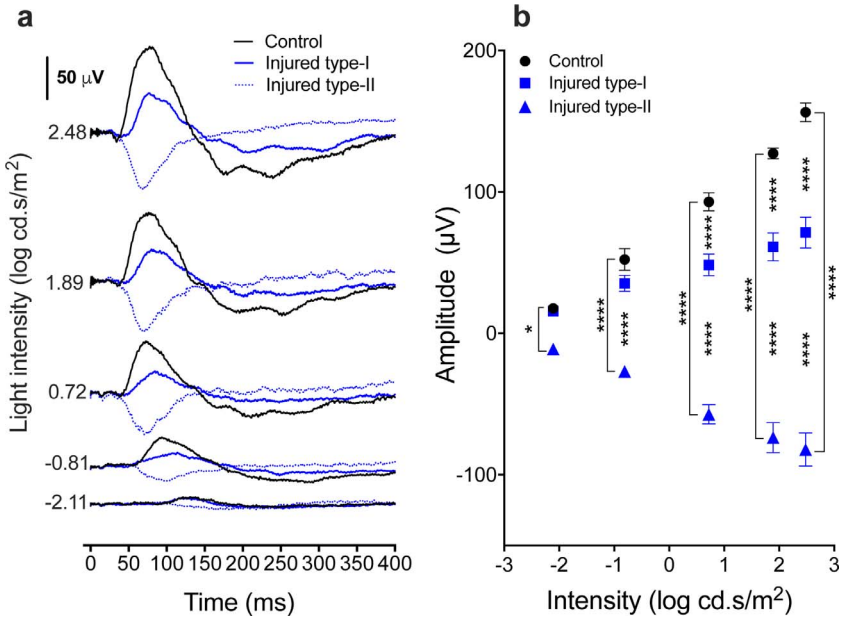

FIGURE 3. Scotopic ERG of control, type-I, and type-II injured larvae. (**a**) Average ERG traces. Based on ERG phenotypes, injured larvae were classified as type-I with reduced b-waves (*blue solid lines*) or type-II with absent b-waves (*blue dashed lines*) relative to controls (*black lines*). *Scale bar* indicates 50 μV. (**b**) ERG amplitude at a fixed time of 70 ms for control (*black discs*), type-I (*blue squares*), and type-II (*blue triangles*) larvae. *Error bars* show ±SEM. In both figure parts, there were 11 control, 11 type-I, and 6 type-II larvae. $^{*}P < 0.05$; $^{****}P < 0.0001$.

after ablation, leading to the loss of connections between photoreceptors and ON-bipolar cells. Accordingly, during ERG measurements, the photoreceptors would hyperpolarize (generating an intact negative a-wave), but the signal would not be relayed to bipolar cells for depolarization (resulting in a reduced or absent b-wave).[18,60] In the case of type-II larvae, where the b-wave is markedly reduced or absent, the negative photoreceptoral responses (a-wave) are fully exposed (Fig. 3a, injured type-II), presenting a remarkably larger trough of ERG signal. Additionally, our ERG recordings do not reveal a large a-wave in normal zebrafish larvae. The brightest light level used is a log unit higher than previous studies reported; thus we conclude that for a typical larval zebrafish ERG waveform, a-waves are small as previously indicated.[14,61,62] However, upon exposure of the full a-wave following b-wave loss in the type-II injured fish, there is a close correspondence between the leading edge of the a-waves of control and injured fish. Therefore, we believe that the injury in this model is largely postreceptoral in nature.

Notably, behavioral and ERG deficits were overall not associated with reduction in bipolar cell numbers (Figs. 4a–c*). It appears that horizontal cell loss in zebrafish did not lead to ON-bipolar cell death, as was the case in horizontal cell–ablated mice.[59] Thus, ERG changes in injured larvae more likely resulted from either moderate (type-I) or severe (type-II) disruption of signaling between photoreceptors and bipolar cells. Abnormal signaling could arise from physical disconnection between photoreceptors and ON-bipolar cells, as described above.[57,58] Alternatively, it may be caused by dysfunction of receptors and signaling molecules on ON-bipolar cells, resulting either directly from horizontal cell ablation or as a developmental consequence. As our injury was induced in larvae at 3 dpf, disruption of horizontal cells at this time may result in abnormal development of photoreceptor and bipolar cell connectivity before experiments at 7 dpf. It is also possible that changes to inhibitory processes, particularly those associated with loss of GABAc input, lead to attenuation of the ERG b-wave.[63]

The complete absence of a b-wave in some injured larvae is similar to the murine no b-wave (nob) models (e.g., TRPM1 or LRIT-3 knockout mice),[64,65] in which signaling through the metabotropic glutamate receptor 6 (mGluR6) cascade on ON-bipolar cell dendrites is disrupted. Loss of the b-wave can occur due to abnormalities in the transient receptor potential M1 (TRPM1) ion channel, which is the endpoint of the mGluR6 cascade.[66,67] In addition, abnormalities in the leucine-rich repeat, lg-like, and transmembrane domains 3 (LRIT-3) protein lead to failure of TRPM1 localization on ON-bipolar dendrites.[68] Whether horizontal cell ablation also impacts receptor localization and/or channel expression requires further functional investigation and labeling for relevant ON-channel proteins (e.g., mGluR6, TRPM1, and LRIT-3).[64–69]

Our ERG results revealed two distinct injury phenotypes, which were associated with different degrees of attenuation in retinal and IPL thickness. There was considerable variation in the number of *Ptf1a*+ neurons—and thus the number of cells expressing the transgenic construct—in control larvae (Fig. 4d). Presumably, nitroreductase expression also differed between larvae before injury, after which retinae that initially expressed more nitroreductase suffered more severe inhibitory neuron loss. Differences between type-I and type-II larvae might thus reflect a dosage effect; this could occur if nitroreductase expression differs between larvae heterozygous and homozygous for the transgene. As ERG differences became apparent only after analysis, we could not retrospectively correlate the ERG against the genotype. While there appears to be a bimodal distribution for both the ERG phenotype (Supplementary Fig. S2) and retinal size (Fig. 4e), it is possible that a larger sample would reveal a more gradual transition of functional difference between groups, as was the case with some of our anatomical measures (e.g., IPL thickness, Fig. 4f). Our results nevertheless indicate that larvae with smaller retinae and thinner IPLs have reduced and in some cases absent ERG b-waves.

Given that horizontal cell ablation appears to have little impact on IPL structure,[58] the reduced IPL thickness we

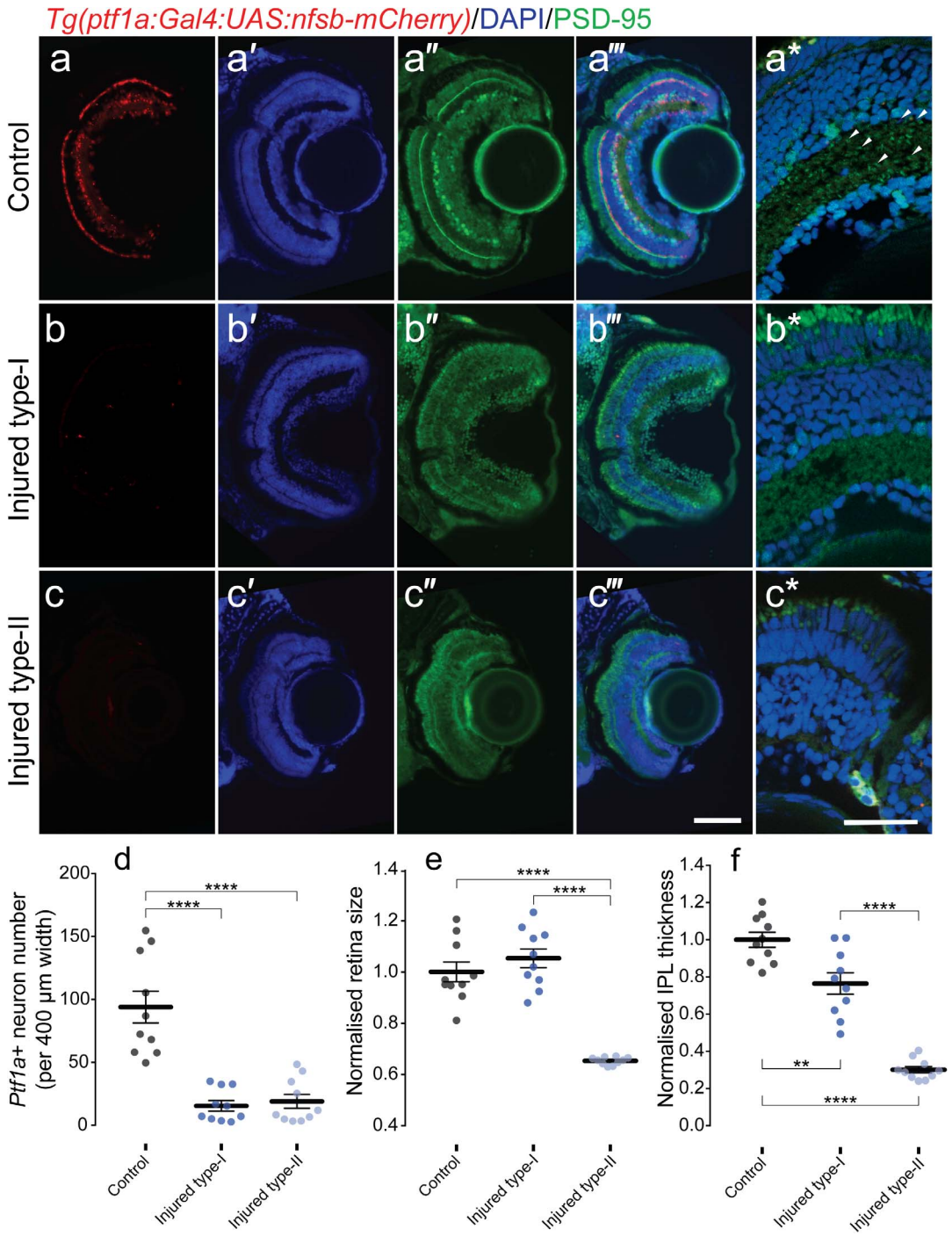

Figure 4. Anatomical phenotype in control versus inhibitory neuron–ablated retinae. (**a–c**) Micrographs of retinal sections from (**a**) control, (**b**) type-I injured, and (**c**) type-II injured larvae labeled by *ptf1a:Gal4/UAS:nfsb-mCherry* (*red*) for inhibitory neurons, DAPI (*blue*) for nuclei, and PSD-95 (*green*) for synapses. Merged images of individual channel images in the left three columns are shown in the fourth column (**a‴**, **b‴**, **c‴**). Apotome merged images at high-power view (**a***, **b***, **c***) are presented for better comparison of the PSD-95 puncta density in the rightmost column. *Scale bar* (**c‴**) for (**a–a‴**, **b–b‴**, **c–c‴**) = 100 µm. *Scale bar* (**c***) for (**a***, **b***, **c***) = 25 µm. (**b**) *Ptf1a*+ neuron number per 400-µm retinal width, (**e**) normalized retinal size, and (**f**) normalized IPL thickness were quantified ($N = 10$ per group). One-way ANOVA was performed. $^{*}P < 0.05$; $^{**}P < 0.01$; $^{***}P < 0.001$; $^{****}P < 0.0001$. *Error bars* show ± SEM.

observed may be due to the loss of inhibitory amacrine cells.[70] Mirroring the effect of horizontal cell ablation in the OPL, the loss of amacrine cells likely interrupts signaling between bipolar, ganglion, and other amacrine cells, causing synaptic disorganization and reducing the size of the IPL. Such reorganization would substantially disrupt ganglion cell receptive fields, affecting spatial vison and motion perception.[71] In mice, ablating starburst amacrine cells abolished ganglion cell directional selectivity and the optokinetic response,[72] while ablating neuropeptide-Y-expressing amacrine cells altered ganglion cell spatial tuning.[73] These inner retinal changes may explain the OMR deficits in our injured larvae. Alterna-

tively, they may be attributable to disruption of visual processing in the outer retina due to horizontal cell loss. To distinguish between additive versus flow-on effects of horizontal and amacrine cell ablation, future experiments might specifically ablate horizontal cells genetically using specific promotors (e.g., connexin57), or chemically through intraocular injection of kainic acid.[57,59]

Both OMR and ERG have advantages and limitations. In combination with anatomical data, the unique strengths of the two methods provide a more complete understanding of visual mechanisms. Unlike the ERG, the OMR allows analyses of spatial vision and higher-order visual perception in larval zebrafish.[8,16] Though spatial contrast sensitivity can also be measured using pattern ERG (pERG) in humans,[74] we are unaware of any successful application of pERG to zebrafish larval eyes, which may in fact be too small for pERG measurements. The OMR measures visual behavior that relies on coordination between different CNS tissues, reflecting the combined activity of complex circuits and networks.[75] For work focused specifically on the retina, alternative explanations for changes in the OMR must be carefully considered, especially when target genes, cell types, or diseases are not visually specific. In our case, because *Ptf1a* gene expression is not specific to retinal inhibitory neurons,[36–38] we turned to locomotor assays to identify any potential confounding factors with large phenotypic effects. In contrast, the ERG is retina-specific and can determine functional integrity of neuronal subtypes through analysis of different ERG components. Throughput also differs substantially between OMR and ERG: OMR analyzes a larger number of larvae simultaneously, but this likely obscures variability between rapidly developing individuals. Compared to OMR, the ERG can be recorded from only one larva at a time, but gives individualized functional insight into retinal deficits, which can identify distinct phenotypes within a group. Anatomical analysis provides subcellular and cellular information from individual retinae in even more detail, but compared to ERG and OMR is invasive and relatively time-consuming. Only by combining results across the three levels of anatomy, physiology, and behavior, can we obtain a comprehensive characterization of the visual phenotype. This analysis paradigm could readily be adapted to other vertebrate models.

Acknowledgments

The authors thank the staff from the zebrafish facility at the Walter and Eliza Hall Institute of Medical Research for animal maintenance. Supported by a grant from the Melbourne Neuroscience Institute (to PTG, PRJ, BVB). PTG was supported by a Discovery Early Career Researcher Award from the Australian Research Council (DE160100125).

Disclosure: **J. Xie**, None; **P.T. Goodbourn**, None; **B.V. Bui**, None; **T.E. Sztal**, None; **P.R. Jusuf**, None

References

1. Gestri G, Link BA, Neuhauss SC. The visual system of zebrafish and its use to model human ocular diseases. *Dev Neurobiol*. 2012;72:302–327.
2. Fadool JM, Dowling JE. Zebrafish: a model system for the study of eye genetics. *Prog Retin Eye Res*. 2008;27:89–110.
3. MacRae CA, Peterson RT. Zebrafish as tools for drug discovery. *Nat Rev Drug Discov*. 2015;14:721–731.
4. Howe K, Clark MD, Torroja CF, et al. The zebrafish reference genome sequence and its relationship to the human genome. *Nature*. 2013;496:498–503.
5. Bilotta J, Saszik S. The zebrafish as a model visual system. *Int J Dev Neurosci*. 2001;19:621–629.
6. Easter JSS, Nicola GN. The development of vision in the zebrafish (Danio rerio). *Dev Biol*. 1996;180:646–663.
7. Orger MB, Baier H. Channeling of red and green cone inputs to the zebrafish optomotor response. *Vis Neurosci*. 2005;22:275–281.
8. Maaswinkel H, Li L. Spatio-temporal frequency characteristics of the optomotor response in zebrafish. *Vision Res*. 2003;43:21–30.
9. Bilotta J. Effects of abnormal lighting on the development of zebrafish visual behavior. *Behav Brain Res*. 2000;116:81–87.
10. Orger MB, Gahtan E, Muto A, Page-McCaw P, Smear MC, Baier H. Behavioral screening assays in zebrafish. *Methods Cell Biol*. 2004:53–68.
11. Niklaus S, Kirla KT, Kraemer T, Groh K, Schirmer K, Neuhauss SC. Cocaine accumulation in zebrafish eyes leads to augmented amplitudes in the electroretinogram. *Matters*. 2017;3:e201703000003.
12. Emran F, Rihel J, Adolph AR, Dowling JE. Zebrafish larvae lose vision at night. *Proc Natl Acad Sci U S A*. 2010;107:6034–6039.
13. Bilotta J, Saszik S, Sutherland SE. Rod contributions to the electroretinogram of the dark-adapted developing zebrafish. *Dev Dyn*. 2001;222:564–570.
14. Saszik S, Bilotta J, Givin CM. ERG assessment of zebrafish retinal development. *Vis Neurosci*. 1999;16:881–888.
15. Xie J, Jusuf PR, Goodbourn PT, Bui BV. Electroretinogram recording in larval zebrafish using a novel cone-shaped sponge-tip electrode. *J Vis Exp*. 2019;145:e59487.
16. Orger MB, Smear MC, Anstis SM, Baier H. Perception of Fourier and non-Fourier motion by larval zebrafish. *Nat Neurosci*. 2000;3:1128.
17. Neuhauss SC, Biehlmaier O, Seeliger MW, et al. Genetic disorders of vision revealed by a behavioral screen of 400 essential loci in zebrafish. *J Neurosci*. 1999;19:8603–8615.
18. Perlman I. The electroretinogram: ERG by Ido Perlman. In: Kolb H, Nelson R, Fernandez E, Jones B, eds. *Webvision: The Organization of the Retina and Visual System*; 2015. Available at: https://webvision.med.utah.edu/.
19. Bateup HS, Johnson CA, Denefrio CL, Saulnier JL, Kornacker K, Sabatini BL. Excitatory/inhibitory synaptic imbalance leads to hippocampal hyperexcitability in mouse models of tuberous sclerosis. *Neuron*. 2013;78:510–522.
20. Hashimoto T, Bergen SE, Nguyen QL, et al. Relationship of brain-derived neurotrophic factor and its receptor TrkB to altered inhibitory prefrontal circuitry in schizophrenia. *J Neurosci*. 2005;25:372–383.
21. Galanopoulou AS. Mutations affecting GABAergic signaling in seizures and epilepsy. *Pflugers Arch*. 2010;460:505–523.
22. Masuda F, Nakajima S, Miyazaki T, et al. Motor cortex excitability and inhibitory imbalance in autism spectrum disorder assessed with transcranial magnetic stimulation: a systematic review. *Transl Psychiatry*. 2019;9:110.
23. Heckers S, Konradi C. GABAergic mechanisms of hippocampal hyperactivity in schizophrenia. *Schizophr Res*. 2015;167:4–11.
24. Kolb H. How the retina works. *Am Sci*. 2003;91:28–35.
25. Dacey DM, Diller LC, Verweij J, Williams DR. Physiology of L- and M-cone inputs to H1 horizontal cells in the primate retina. *J Opt Soc Am A Opt Image Sci Vis*. 2000;17:589–596.
26. Zhang A-J, Wu SM. Receptive fields of retinal bipolar cells are mediated by heterogeneous synaptic circuitry. *J Neurosci*. 2009;29:789–797.

27. Mangel SC. Analysis of the horizontal cell contribution to the receptive field surround of ganglion cells in the rabbit retina. *J Physiol*. 1991;442:211–234.
28. Lankheet MJM, Van Wezel RJA, Prickaerts JHHJ, Van De Grind WA. The dynamics of light adaptation in cat horizontal cell responses. *Vision Res*. 1993;33:1153–1171.
29. Smith RG, Vardi N. Simulation of the Aii amacrine cell of mammalian retina: functional consequences of electrical coupling and regenerative membrane properties. *Vis Neurosci*. 1995;12:851–860.
30. Demb JB, Singer JH. Intrinsic properties and functional circuitry of the AII amacrine cell. *Vis Neurosci*. 2012;29:51–60.
31. Lasater EM, Dowling JE. Dopamine decreases conductance of the electrical junctions between cultured retinal horizontal cells. *Proc Natl Acad Sci U S A*. 1985;82:3025–3029.
32. He S, Weiler R, Vaney DI. Endogenous dopaminergic regulation of horizontal cell coupling in the mammalian retina. *J Comp Neurol*. 2000;418:33–40.
33. Curado S, Stainier DY, Anderson RM. Nitroreductase-mediated cell/tissue ablation in zebrafish: a spatially and temporally controlled ablation method with applications in developmental and regeneration studies. *Nat Protoc*. 2008;3:948–954.
34. Ng Chi Kei J, Currie PD, Jusuf PR. Fate bias during neural regeneration adjusts dynamically without recapitulating developmental fate progression. *Neural Dev*. 2017;12:12.
35. Jusuf PR, Harris WA. Ptf1a is expressed transiently in all types of amacrine cells in the embryonic zebrafish retina. *Neural Dev*. 2009;4:34.
36. Hoshino M, Nakamura S, Mori K, et al. Ptf1a, a bHLH transcriptional gene, defines GABAergic neuronal fates in cerebellum. *Neuron*. 2005;47:201–213.
37. Glasgow SM, Henke RM, MacDonald RJ, Wright CV, Johnson JE. Ptf1a determines GABAergic over glutamatergic neuronal cell fate in the spinal cord dorsal horn. *Development*. 2005;132:5461–5469.
38. Hoshino M. Molecular machinery governing GABAergic neuron specification in the cerebellum. *Cerebellum*. 2006;5:193–198.
39. Jusuf PR, Almeida AD, Randlett O, Joubin K, Poggi L, Harris WA. Origin and determination of inhibitory cell lineages in the vertebrate retina. *J Neurosci*. 2011;31:2549–2562.
40. Bizrah M, Dakin SC, Guo L, et al. A semi-automated technique for labeling and counting of apoptosing retinal cells. *BMC Bioinformatics*. 2014;15:169.
41. Lu Z-L, Dosher B. *Visual Psychophysics: From Laboratory to Theory*. Cambridge, MA: MIT Press; 2013.
42. Sztal TE, Ruparelia AA, Williams C, Bryson-Richardson RJ. Using touch-evoked response and locomotion assays to assess muscle performance and function in zebrafish. *J Vis Exp*. 2016;116:e54431.
43. El-Husseini AE-D, Schnell E, Dakoji S, et al. Synaptic strength regulated by palmitate cycling on PSD-95. *Cell*. 2002;108:849–863.
44. Schindelin J, Arganda-Carreras I, Frise E, et al. Fiji: an open-source platform for biological-image analysis. *Nat Methods*. 2012;9:676.
45. Botta P, de Souza FMS, Sangrey T, De Schutter E, Valenzuela CF. Alcohol excites cerebellar golgi cells by inhibiting the Na+/K+ ATPase. *Neuropsychopharmacology*. 2010;35:1984.
46. Lockwood B, Bjerke S, Kobayashi K, Guo S. Acute effects of alcohol on larval zebrafish: a genetic system for large-scale screening. *Pharmacol Biochem Behav*. 2004;77:647–654.
47. Pardue MT, Peachey NS. Mouse b-wave mutants. *Doc Ophthalmol*. 2014;128:77–89.
48. Wang K, Hinz J, Zhang Y, Thiele TR, Arrenberg A. Parallel channels for motion feature extraction in the pretectum and tectum of larval zebrafish [published online ahead of print August 26, 2019]. *Cell Rep*. http://dx.doi.org/10.2139/ssrn.3443147.
49. Mueller T, Vernier P, Wullimann MF. A phylotypic stage in vertebrate brain development: GABA cell patterns in zebrafish compared with mouse. *J Comp Neurol*. 2006;494:620–634.
50. Thalman C, Horta G, Qiao L, et al. Synaptic phospholipids as a new target for cortical hyperexcitability and E/I balance in psychiatric disorders. *Mol Psychiatry*. 2018;23:1699–1710.
51. Yizhar O, Fenno LE, Prigge M, et al. Neocortical excitation/inhibition balance in information processing and social dysfunction. *Nature*. 2011;477:171.
52. Selimbeyoglu A, Kim CK, Inoue M, et al. Modulation of prefrontal cortex excitation/inhibition balance rescues social behavior in *CNTNAP2*-deficient mice. *Sci Transl Med*. 2017;9:eaah6733.
53. Ferguson BR, Gao W-J. PV interneurons: critical regulators of E/I balance for prefrontal cortex-dependent behavior and psychiatric disorders. *Front Neural Circuits*. 2018;12:37.
54. Kim YS, Woo J, Lee CJ, Yoon B-E. Decreased glial GABA and tonic inhibition in cerebellum of mouse model for attention-deficit/hyperactivity disorder (ADHD). *Exp Neurobiol*. 2017;26:206–212.
55. Rubenstein JLR, Merzenich MM. Model of autism: increased ratio of excitation/inhibition in key neural systems. *Genes Brain Behav*. 2003;2:255–267.
56. Schneider P, Petzold S, Sommer A, et al. Altered synaptic phospholipid signaling in PRG-1 deficient mice induces exploratory behavior and motor hyperactivity resembling psychiatric disorders. *Behav Brain Res*. 2018;336:1–7.
57. Messersmith EK, Redburn DA. Kainic acid lesioning alters development of the outer plexiform layer in neonatal rabbit retina. *Int J Dev Neurosci*. 1990;8:447–461.
58. Hammang JP, Behringer RR, Baetge EE, Palmiter RD, Brinster RL, Messing A. Oncogene expression in retinal horizontal cells of transgenic mice results in a cascade of neurodegeneration. *Neuron*. 1993;10:1197–1209.
59. Sonntag S, Dedek K, Dorgau B, et al. Ablation of retinal horizontal cells from adult mice leads to rod degeneration and remodeling in the outer retina. *J Neurosci*. 2012;32:10713–10724.
60. McCall MA, Gregg RG. Comparisons of structural and functional abnormalities in mouse b-wave mutants. *J Physiol*. 2008;586:4385–4392.
61. Seeliger MW, Rilk A, Neuhauss SC. Ganzfeld ERG in zebrafish larvae. *Doc Ophthalmol*. 2002;104:57–68.
62. Chrispell JD, Rebrik TI, Weiss ER. Electroretinogram analysis of the visual response in zebrafish larvae. *J Vis Exp*. 2015;97:e52662.
63. Kapousta-Bruneau NV. Opposite effects of GABAA and GABAC receptor antagonists on the b-wave of ERG recorded from the isolated rat retina. *Vision Res*. 2000;40:1653–1665.
64. Morgans CW, Zhang J, Jeffrey BG, et al. TRPM1 is required for the depolarizing light response in retinal ON-bipolar cells. *Proc Natl Acad Sci U S A*. 2009;106:19174–19178.
65. Neuillé M, El Shamieh S, Orhan E, et al. Lrit3 deficient mouse (nob6): a novel model of complete congenital stationary night blindness (cCSNB). *PLoS One*. 2014;9:e90342.
66. Morgans CW, Brown RL, Duvoisin RM. TRPM1: the endpoint of the mGluR6 signal transduction cascade in retinal ON-bipolar cells. *Bioessays*. 2010;32:609–614.
67. Morgans CW. All ON pathways are not alike. *J Physiol*. 2015;593:1527–1528.

Investigative Ophthalmology & Visual Science

68. Neuillé M, Morgans CW, Cao Y, et al. LRIT3 is essential to localize TRPM1 to the dendritic tips of depolarizing bipolar cells and may play a role in cone synapse formation. *Eur J Neurosci*. 2015;42:1966–1975.
69. Zhang RW, Du JL. In vivo whole-cell patch-clamp recording in the zebrafish brain. In: Kawakami K, EE, Patton Orger M, eds. *Zebrafish: Methods and Protocols*. New York, NY: Springer New York; 2016:281–291.
70. Reese BE, Raven MA, Giannotti KA, Johnson PT. Development of cholinergic amacrine cell stratification in the ferret retina and the effects of early excitotoxic ablation. *Vis Neurosci*. 2001;18:559–570.
71. Wienbar S, Schwartz GW. The dynamic receptive fields of retinal ganglion cells. *Prog Retin Eye Res*. 2018;67:102–117.
72. Yoshida K, Watanabe D, Ishikane H, Tachibana M, Pastan I, Nakanishi S. A key tole of starburst amacrine cells in originating retinal directional selectivity and optokinetic eye movement. *Neuron*. 2001;30:771–780.
73. Sinclair JR, Jacobs AL, Nirenberg S. Selective ablation of a class of amacrine cells alters spatial processing in the retina. *J Neurosci*. 2004;24:1459–1467.
74. Berninger T, Schuurmans RP. Spatial tuning of the pattern ERG across temporal frequency. *Doc Ophthalmol*. 1985;61:17–25.
75. Naumann EA, Fitzgerald JE, Dunn TW, Rihel J, Sompolinsky H, Engert F. From whole–brain data to functional circuit models: the zebrafish optomotor response. *Cell*. 2016;167:947–960.

Investigative Ophthalmology & Visual Science